Karsili, T. N. V., Marchetti, B., Moca, R., & Ashfold, M. N. R. (2013). UV Photodissociation of Pyrroles: Symmetry and Substituent Effects. The Journal of Physical Chemistry A, 117(46), 12067-12074. 10.1021/jp404580v

UV Photodissociation of Pyrroles; Symmetry and Substituent Effects

Tolga N.V. Karsili, Barbara Marchetti, Roberta Moca[#] and Michael N.R. Ashfold[*]

School of Chemistry, University of Bristol, Cantock's Close, Bristol, BS8 1TS

No. of Figures: 8

No. of Tables: 2

Supplementary Information. 3 Figures and 1 Table

* Corresponding author

Professor M.N.R. Ashfold

(address as above)

mike.ashfold@bris.ac.uk

Tel: +44 (117) 928 8312

[#]Present address: School of Chemistry, Faculty of Science, University of East Anglia, Norwich Research Park, Norwich, NR4 7TJ, UK

Keywords

Photofragmentation dynamics, gas phase, πσ* excited states, conical intersections.

Abstract

H (Rydberg) atom photofragment translational spectroscopy and *ab initio* electronic structure calculations are used to explore ways in which ring substituents affect the photofragmentation dynamics of gas phase pyrroles. $S_1 \leftarrow S_0$ ($\sigma^* \leftarrow \pi$) excitation in bare pyrrole is electric dipole forbidden, but gains transition probability by vibronic mixing with higher electronic states. The S_1 state is dissociative with respect to N–H bond extension, and the resulting pyrrolyl radicals are formed in a limited number of (non-totally symmetric) vibrational levels (Cronin *et al*. *Phys. Chem. Chem. Phys.* **2004**, *6*, 5031-5041). Introducing σ-perturbing groups (*e.g*. an ethyl group in the 2-position, or methyl groups in the 2- and 4-positions) lowers the molecular symmetry (to C_s), renders the S_1–S_0 transition (weakly) allowed and causes some reduction in N–H bond strength; the radical products are again formed in a select sub-set of the many possible vibrational levels, but all involve in-plane (*a′*) ring-breathing motions as expected (by Franck-Condon arguments) given the changes in equilibrium geometry upon $\sigma^* \leftarrow \pi$ excitation. The effects of π-perturbers are explored computationally only. Relative to bare pyrrole, introducing an electron donating group like methoxy (at the 3- or, particularly, the 2-position) is calculated to cause a ~10% reduction in N–H bond strength, while CN substitution (in either position) is predicted to cause a substantial (~3000 cm^{-1}) increase in the S_1–S_0 energy separation but only a modest (~2%) increase in N–H bond strength.

1. INTRODUCTION

X–H bond fission is now recognized as a significant decay pathway following electronic excitation of many heteroatom containing aromatic molecules, including small azoles like pyrrole, imidazole, *etc*, larger analogues like indoles and adenine, and many phenols and thiophenols. These systems serve to illustrate the importance of (n/π)σ* excited states (*i.e.* excited states formed via σ*←n or σ*←π electron promotions) in promoting such bond fissions, and much recent research has sought to explore the importance (or otherwise) of such processes following UV photoexcitation of larger, more biochemically relevant molecules.[1-4] Increasing size is accompanied by an increase in the vibrational (and in many cases electronic) state density and, typically, in the number and efficiency of alternative, radiationless, pathways by which excited state population can be channeled back to the ground (S_0) electronic state.[5-8]

Here we revisit the primary photochemistry of pyrroles, and report the first studies of the effects of introducing ring substitutents that break the C_{2v} parent symmetry. Photofragment translational spectroscopy (PTS) experiments by Lee and coworkers[9] demonstrated N–H bond fission following 248 nm excitation of bare pyrrole; the measured total kinetic energy release (TKER) of the H + pyrrolyl products was consistent with (vibronically induced) excitation from the highest occupied molecular orbital (HOMO, π(a_2)) to the lowest unoccupied molecular orbital (LUMO, σ*(a_1)), and prompt dissociation on the excited ^{1}πσ* potential energy surface (PES). This interpretation was validated by the electronic structure calculations of Sobolewski and Domcke,[10] which served to trigger the growing recognition of the importance of πσ* PESs in excited state photochemistry. This work also highlighted the conical intersection (CI) between the S_1(^{1}πσ*) and S_0 state PESs at extended N–H bond lengths ($R_{N–H}$); at planar geometries, the S_1 and S_0 states correlate diabatically with,

respectively, the ground ($^2A_2$) and second excited ($^2A_1$) states of the pyrrolyl radical (plus an H atom in each case). Subsequent calculations [11] identified a second $^1\pi\sigma^*$ state (the $S_2(^1B_1)$ state, correlating to a low lying $^2B_1$ excited state of the radical), the PES for which displays similar topology to that of the S_1 state along R_{N-H} and, at slightly higher energy, two $^1\pi\pi^*$ excited states (the $S_3(^1B_2)$ and $S_4(^1A_1)$ states), the PESs for which are bound in all coordinates.

The $S_1 \leftarrow S_0$ ($^1A_2 – X^1A_1$) transition in pyrrole is electric dipole forbidden, but gains (weak) oscillator strength by vibronic mixing with allowed transitions to higher excited states.[12] The early PTS result was confirmed by a velocity map imaging (VMI) study of the H atoms from pyrrole photolysis at λ = 243.1 nm.[13, 14] Higher resolution TKER spectra of the H + pyrrolyl fragments formed following near UV excitation to the S_1 state of pyrrole show structure attributable to population of specific vibrational levels of the radical product.[15, 16] The relative branching into these levels varies with photolysis wavelength, but all of the populated levels (apart from the v = 0 level) are found to involve non-totally symmetric nuclear motions. The product energy disposals and recoil anisotropies have been rationalised in terms of vibronically induced $S_1 \leftarrow S_0$ excitation, followed by prompt N–H bond fission – a view confirmed in a number of ultrafast pump-probe studies.[17-19] The skeletal motions that promote vibronic coupling with the off-resonant excited electronic state (or states) are orthogonal to the dissociation coordinate and thus act as 'spectators' to the bond fission process, mapping through relatively unchanged into the corresponding vibrational motion in the eventual radical fragment. The formation of v = 0 products implies that at least one of the parent modes lost on N–H bond fission (*e.g.* the out-of-plane NH wag (b_1 symmetry in C_{2v})) also promotes coupling to a higher electronic state.[15] $S_2 \leftarrow S_0$ ($\sigma^* \leftarrow \pi$) excitation must make an increasing contribution upon tuning to shorter wavelengths, but the vibrational structure

evident in the TKER spectra of the H + pyrrolyl fragments (and D + pyrrolyl-d_4 fragments from photolysis of pyrrole-d_5 [20]) have been interpreted simply in terms of X state radical formation (probably as a result of strong vibronic mixing between the X^2A_2 and first excited $^2B_1$ electronic states of the radical [21,22]). TKER spectra recorded at yet shorter wavelengths (λ ~210 nm), where excitation is to the $^1\pi\pi^*(^1B_2)$ state, are clearly bimodal. A broad feature, displaying preferential perpendicular recoil anisotropy and centred at similar TKER (~6000 cm^{-1}) to that found when exciting the $^1\pi\sigma^*$ state(s) directly, is attributed to efficient radiationless transfer to one or other or both of the $^1\pi\sigma^*$ PESs and subsequent prompt dissociation to H + pyrrolyl products, while a second, isotropic, feature peaking at low TKER is attributed to unimolecular decay of internally 'hot' parent molecules formed via radiationless transfer to the S_0 state. Subsequent non-adiabatic dynamics calculations using a surface hopping approach at the time dependent density functional level of theory provide broad support for this picture.[23]

The present study builds on this prior work in two ways. Experimentally, we show that breaking the C_{2v} symmetry of pyrrole (by substituting an ethyl group in the 2-position or by introducing methyl (Me) groups at the 2- and 4-positions) leads to a quantitatively different vibrational energy disposal in the radical fragments formed upon N–H bond fission. The experimental measurements are complemented by electronic structure calculations, that compare and contrast the photofragmentation behavior of pyrrole with not just 2-ethylpyrrole (2-EP) and 2,4-dimethylpyrrole (2,4-DMP), but also with 2- and 3-methoxypyrrole and 2- and 3-cyanopyrrole. In each case, the substituent lowers the molecular symmetry *cf*. bare pyrrole, but the electronic perturbations they cause are very different. The alkyl groups are relative mild perturbers of the σ-framework, whereas the cyano- (CN-) and methoxy- (MeO-) substituents respectively withdraw electron density from, and donate electron density to, the

ring π-system. Each is shown to have a distinctive and, to a large extent, predictable effect on the parent excitation spectrum and the ensuing fragmentation dynamics.

2. METHODS

2.1 Experimental

The design and operation of the H Rydberg atom PTS experiment has been described previously.[15,24] In brief, the apparatus comprises two differentially pumped volumes (a source chamber (base pressure, p ~2 x 10^{-6} mbar) and a detection chamber (p ~6 x 10^{-8} mbar) that incorporates the interaction region) separated by a skimmer. The 2-EP and 2,4-DMP samples (Sigma Aldrich (purity >99%)) were seeded in ~1 bar of Ar, expanded in the form of a pulsed molecular beam and skimmed before being intersected by a pulsed photolysis laser beam. Both samples are liquids at room temperature. In the case of 2,4-DMP, adequate signal levels were obtainable using its room temperature vapour pressure, but in the case of 2-EP it was necessary to place some of the liquid in an inline filter positioned close behind the pulsed valve and maintained at ~35°C. The H atom photoproducts were 'tagged' by two photon (121.6 nm + 366 nm) double resonant excitation *via* the 2*p* state to Rydberg states with principle quantum number n ~80, and their times-of-flight (TOFs) to a detector positioned along an axis orthogonal to the plane containing the molecular and laser beams measured. Recoil anisotropies were determined by comparing spectra recorded with the polarisation vector ($\boldsymbol{\varepsilon}_{\mathbf{phot}}$) of the photolysis laser radiation aligned at θ = 0°, 90° and 54.7° to the TOF axis.

2.2 Computational

A range of methods were used to explore selected properties of the substituted pyrroles considered in this work. The ground state minimum energy geometry of each molecule was optimised using Møller-Plesset second order perturbation (MP2) theory along with Dunning's augmented correlation consistent basis set of triple ζ quality: aug-cc-pVTZ using the Gaussian 09 Computational package[25]. Vertical excitation energies and transition dipole moments (TDMs) to the first four singlet excited states were calculated using a state averaged complete active space self-consistent field (SA-CASSCF) method with the aug-cc-pVTZ basis set with extra even tempered sets of *s* and *p* diffuse functions to describe the Rydberg-valance mixing more effectively (henceforth referred to as aug(N)-AVTZ). An active space comprising 10 electrons in 10 orbitals as follows: the three ring-centred π bonding orbitals and the two π* antibonding orbitals, the N centered 3s Rydberg orbital and two occupied σ and two virtual σ* orbitals, one of each of which is localised around the N–H bond. Potential energy cuts (PECs) along $R_{N–H}$ were calculated for the ground and first two $^1\pi\sigma^*$ states using complete active space with second order perturbation theory (CASPT2) based on a fully SA-CASSCF reference wavefunction, with the remainder of the nuclear framework frozen at the optimised ground state geometry. A small imaginary level shift of 0.5 a.u. was applied in all cases to encourage convergence and to circumvent the presence of intruder states. Equation of motion coupled cluster single and double (EOM-CCSD) calculations were also performed at the MP2 optimized ground state geometry with the aug(N)-AVTZ basis set to calculate the vertical excitation energies, TDM vectors and associated oscillator strengths (*f*) for transitions from S_0 to the $S_1$and $S_2(^1\pi\sigma^*)$ states and the S_3 and $S_4(^1\pi\pi^*)$ states. The above calculations were all performed using MOLPRO Version 2010.1.[26]

In the specific case of 2-EP, PECs were also calculated along the ethyl torsional coordinate in order to determine the minimum energy geometries and relative stabilities of the parent S_0

and S_1 states and the ground (D_0) state of the radical. The torsion angle (ϕ) is defined with respect to torsion about the C(2)–CH_2CH_3 bond. PECs were calculated from $\phi = 0°$ (where the terminal CH_3 carbon eclipses the N atom) to $\phi = 180°$ in steps of 15°. The S_0 PEC was calculated at the DFT/B3LYP/6-311+G(*d,p*) level of theory, using Gaussian 09 [25] and allowing the rest of the nuclear framework to relax at each value of ϕ. The torsional PEC for the D_0 state of the radical was calculated in the same way, while that for the parent S_1 state was calculated using time dependent (TD-) DFT, again using the B3LYP functional and the 6-311+G(*d*, *p*) basis set.

Anharmonic wavenumbers for the ground states of pyrrole, 2-EP and 2,4-DMP and of the corresponding radicals formed by N–H bond fission were similarly calculated at the DFT/B3LYP/6-311+G(*d*, *p*) level of theory. The same functional and basis set were also used to explore the effects of π substituents, at both the 2- and 3-positions. Molecules chosen for investigation were 2- and 3-methoxypyrrole and 2- and 3-cyanopyrrole (*i.e.* pyrroles involving classic π electron donating and withdrawing substituents, respectively), as well as 2-EP, 2,4-DMP and bare pyrrole itself as benchmarks. Quantities determined in each case were: the N–H bond strength (from the (zero-point corrected) energy difference between the ground state molecule and ground state radical); the ionization potential (I.P., from the (zero-point corrected) energy difference between the ground state molecule and the ground state parent cation); and $\Delta E(S_1\text{-}S_0)$. The latter quantity, the vertical energy separation between the S_1 and S_0 states, was calculated using TD-DFT, with the same functional and basis set.

3. RESULTS AND DISCUSSION

3.1 *Ab initio* results for pyrrole, 2-ethylpyrrole and 2,4-dimethylpyrrole

(a) Pyrrole

For orientation, fig. 1 displays unrelaxed CASPT2 PECs along R_{N-H} for the ground and the first two $^1\pi\sigma^*$ excited states of pyrrole. As noted previously,[11] these PECs display shallow minima in the vertical Franck-Condon region (vFC) – a consequence of Rydberg/valence (3s/σ*) interaction, reminiscent of that found in ammonia, *etc*.[27] – and CIs with the S_0 potential at a planar geometry, *en route* to the asymptotic products (the ground and first excited state of the pyrrolyl radical, respectively, and an H atom). The PECs for the S_3 and $S_4(^1\pi\pi^*)$ states are both bound, and lie above those of the $^1\pi\sigma^*$ states.[11]

(b) Substituent effects on the orbitals, excitation energies and oscillator strengths.

Figure 2 compares the nodal properties of the two highest occupied and two lowest unoccupied CASSCF MOs of pyrrole with those of the corresponding orbitals for 2,4-DMP and 2-EP. Breaking the C_{2v} symmetry (as in 2,4-DMP and 2-EP) causes some minor distortion of the orbitals, more evidently in the case of 2,4-DMP, but is not predicted to cause any change in their relative energetic ordering. Table 1 lists calculated vertical excitation energies and oscillator strengths for transitions from the S_0 state to the first four excited singlet states in pyrrole, 2-EP and 2,4-DMP. The dominant orbital promotions behind these various excitations are indicated in fig. 2. As Table 1 shows, 2-alkyl substitution leads to a red-shift in the S_1–S_0 transition; the symmetry lowering is also reflected by the increased oscillator strength of these transitions (*cf*. pyrrole).

(c) Conformers of 2-ethylpyrrole

2-EP displays *anti* and *gauche* conformers in its S_0 state, distinguished by the position of the ethyl CH_3 group relative to the C atom in the ring 3-position (C3). As fig. 3 shows, the

guache-conformer (*i.e.* ϕ ~60°) is calculated to be more stable (by ~90 cm^{-1}) and the conformation with ϕ = 0° corresponds to a saddle point, lying ~500 cm^{-1} above the global minimum. Such stereochemistry is reminiscent of that exhibited by butane, and plausibly attributed to steric factors. Thus we assume that the majority of 2-EP molecules in our molecular beam sample will be in the *gauche*-configuration. The calculated minimum energy geometry of the S_1 state parent molecule (and of the ground state radical), in contrast, occurs at ϕ = 0° (*i.e.* the *syn*-conformer) – presumably the result of some H-bonding between the terminal CH_3 group and the electron density on the N atom. Vertical excitation is thus likely to prepare S_1 molecules with $\phi \neq 0°$ which relax towards the *syn*-conformer during the ensuing N–H bond extension.

(d) PECs along $R_{N–H}$ for the S_0, S_1 and S_2 states of 2,4-dimethylpyrrole

Unrelaxed CASPT2(10/10)/aug(N)-AVTZ PECs for 2,4-DMP, analogous to those for pyrrole shown in fig. 1, are included in the Supplementary Information (fig. S1). The shallow minimum in the S_1 PEC is more developed in 2,4-DMP; the calculated energy barrier in the $R_{N–H}$ coordinate (defined relative to the S_1 minimum in the vFC region) is ~0.35 eV, *cf.* ~0.2 eV in bare pyrrole. Such a trend mirrors that deduced previously in the case of 2,5-DMP [28] and, as in that case, we can anticipate that N–H bond fission following threshold excitation to the lowest (v=0) vibrational level of the S_1 state will involve tunneling through this barrier and subsequent diabatic evolution along the dissociative potential at long range to ground state radical products.

3.2 H atom PTS spectra from 2-ethylpyrrole and 2,4-dimethylpyrrole

H atom TOF spectra of 2-EP and 2,4-DMP were recorded at many photolysis wavelengths (λ_{phot}) in the range $275 > \lambda_{phot} \geq 245$ nm and at 193.3 nm. Each was converted to a TKER spectrum *via* eq. (1):

$$TKER = \frac{1}{2} m_H \left(1 + \frac{m_H}{m_R}\right)\left(\frac{d}{t}\right)^2 \quad (1)$$

where m_H and m_R are, respectively, the masses of the H atom and the radical co-fragment. The latter are assumed to be 2-ethylpyrrolyl (2-EPyl) and 2,4-dimethylpyrrolyl (2,4-DMPyl) in the case of 2-EP and 2,4-DMP, respectively; both radicals have m_R = 94.135 u. d in eq. (1) is the distance between the interaction region and the front face of the detector, and t is the measured H atom TOF. A t^{-3} Jacobian was used to re-bin the measured intensities when converting spectra from the TOF to TKER domain.

(a) 2-Ethylpyrrole

The longest photolysis wavelength at which a measurable H atom yield was discernible was 267 nm (*cf.* 254 nm in the case of bare pyrrole[15]). Figure 4 shows TKER spectra of the H + 2-EPyl products resulting from photolysis of 2-EP at λ_{phot} = (a) 260, (b) 257 and (c) 246 nm. As in the cases of pyrrole and 2,5-DMP,[15,20,27] these spectra display a structured feature centered at TKER ~6000 cm^{-1}, attributable to one-photon induced N–H bond fission and formation of 2-EPyl radicals in selected vibrational levels of the ground electronic state. Analyses of these and many similar spectra yield a value for the N–H bond dissociation energy (D_0[2-EPyl–H]) *via* eq. (2)

$$E_{phot} = \mathrm{TKER}_{max} + D_0[2\text{-EPyl-H}], \quad (2)$$

where E_{phot} is the photolysis photon energy, we have ignored any contribution from the internal energy of the jet-cooled parent molecule and we associate the fastest ($TKER_{max}$) peak in each spectrum with formation of radical products in their zero-point (v = 0) vibrational

level. The best-fit line of unit gradient through a 24-point plot of E_{phot} *vs* $TKER_{max}$ (Supplementary Information, fig. S2) yields a *y*-axis intercept: D_0[2-EPyl–H]) = 31650±50 cm^{-1}. As noted above, we attribute this value to the energy difference between the respective zero-point levels of the *gauche*-conformer of 2-EP and the *syn*-conformer of the 2-EPyl radical. This bond strength is ~1200 cm^{-1} lower than that of the N–H bond in bare pyrrole, consistent with the expected (destabilizing) +*I* inductive effect of alkyl substitution in the 2-position. All of the measured spectra are more intense when $\boldsymbol{\varepsilon_{phot}}$ is aligned perpendicular to the TOF axis (*i.e.* $\theta = 90°$) but the same spectrum can be observed at $\theta = 0°$; the best-fit anisotropy parameter β is ~ –0.6 and independent of TKER. The sign of β is consistent with $S_1 \leftarrow S_0$ excitation (the TDM for which is perpendicular to the ring plane), while the finding that its value is non-limiting may indicate that the (presumed) tunneling step is encouraged by N–H out-of-plane bending motion or, perhaps more probably, that the tunneling timescale is commensurate with that for (partial) parent rotation.

Given D_0[2-EPyl–H]) = 31650±50 cm^{-1}, each TKER spectrum can be recast as a spectrum of radical yield versus internal energy (E_{int})

$$E_{int} = E_{phot} - D_0[2\text{-EPyl-H}]) - \text{TKER} \qquad (3)$$

and thereby provide insight into the ways in which the vibrational excitation of the radical products evolves with excitation energy. Figure 5 shows E_{int} spectra obtained following excitation at various wavelengths in the range $263 \geq \lambda_{phot} \geq 248$ nm. The longest wavelength spectra are dominated by a single peak that we attribute to formation of 2-EPyl radicals in their v=0 level, but a feature at E_{int} ~960 cm^{-1} is clearly evident in fig. 5(b) and other features develop at *e.g.* E_{int} ~1340 cm^{-1} and ~2260 cm^{-1} upon tuning to shorter wavelengths. Reference to the calculated anharmonic wavenumbers of the vibrational modes of the *syn*-

conformer of the 2-EPyl radical (Supplementary Information, Table S1) shows that the 960 cm^{-1} value matches well with one quantum of in-plane radical vibration ν_{20}. Activity in this mode is understandable on Franck-Condon grounds, given that the calculated wavenumber of this mode drops by ~15% on $S_1 \leftarrow S_0$ excitation. Attributing the 1340 cm^{-1} interval is less clear cut, but one quantum of ν_{12} (another in-plane ring breathing motion) is the most plausible interpretation based on the nuclear motions expected as a result of $\sigma^* \leftarrow \pi$ excitation, and we assign it accordingly. The 2260 cm^{-1} interval we assign to the combination $\nu_{12}=1 + \nu_{20}=1$. The nuclear distortions associated with these two modes are depicted in fig. 6. None of these features are as well resolved as in the corresponding spectra from photolysis of bare pyrrole. This likely reflects the spread of torsional energies in the parent molecule and, particularly, the 2-EPyl product given the reorientation of the pendant ethyl group upon dissociation implied by the PECs shown in fig. 3.

The observed product vibrational energy disposals show obvious similarities and differences with those reported previously for bare pyrrole.[15] In both cases, the mean E_{int} value increases with increasing E_{phot} and the identity of the populated product modes (and their dependence on λ_{phot}) suggests a high degree of vibrational adiabaticity in the fragmentation process. Photo-excitation at any given wavelength is assumed to populate one or more lifetime broadened vibronic resonances within the overall $S_1 \leftarrow S_0$ absorption. The 'active' vibrations in both 2-EP and pyrrole are predominantly skeletal motions orthogonal to the dissociation coordinate, *i.e.* 'spectator' modes, which map through into the radical product upon N–H bond fission. What determines the 'active' modes is different in the two cases, however. The $S_1 \leftarrow S_0$ transition in 2-EP is dipole allowed, and the active vibrations are determined by Franck-Condon considerations (*i.e.* by the changes in equilibrium geometry upon photoexcitation, and/or during the evolution from S_1 molecule to the ground state radical).

Hence the propensity for populating in-plane (a') product vibrations, and the uniformity of the measured β values. The $S_1 \leftarrow S_0$ transition in pyrrole, in contrast, is dipole forbidden and the product energy disposal (and recoil anisotropy) reflects the non-totally symmetric parent mode(s) that provide the dominant vibronic transition probability at the λ_{phot} of interest.[15]

(b) 2,4-dimethylpyrrole

The longest photolysis wavelength at which a measurable H atom yield was obtained was 273.4 nm. Illustrative TKER spectra derived from H atom TOF spectra measured following photolysis of 2,4-DMP are shown in the Supplementary Information (fig. S3), along with a 14-point plot of E_{phot} *vs* $TKER_{max}$ from which we determine: D_0[2,4-DMPyl–H]) = 31200±50 cm^{-1}. Again, alkyl substitution is seen to reduce the N–H bond strength relative to that in bare pyrrole. The finding that this reduction is less than in the case of 2,5-DMP (D_0[2,5-DMPyl–H]) = 30530±100 cm^{-1}) [27] serves to reinforce the conclusion that alkyl substitution in the 2- (and 5-) positions causes the greater (destabilizing) +*I* inductive effect. As with 2-EP, the measured spectra are more intense when recorded with $\boldsymbol{\varepsilon_{phot}}$ aligned perpendicular to the TOF axis (*i.e.* at $\theta = 90°$), and the best-fit β value is ~ –0.6.

Given D_0[2,4-DMPyl-H], the TKER spectra can be converted into E_{int} spectra of the radical product (fig. 7). All of the displayed E_{int} spectra reveal formation of radicals in the v=0 level but, again, more of the products appear with progressively greater internal energy upon tuning to shorter photolysis wavelengths and, again, the individual peaks are less well resolved than in the corresponding spectra from photolysis of bare pyrrole. Peaks at E_{int} ~270, ~690, ~945 and ~1300 cm^{-1} are readily identifiable. Reference to Table S1 suggests assignment of these features to population of, respectively, radical modes ν_{25}, ν_{22} and ν_{19} and ν_{14} (as shown in fig. 7). As in 2-EP, the population of such in-plane ring centred modes – the

associated nuclear motions for which are also shown in fig. 6 – can be explained by assuming (i) initial photo-excitation of (Franck-Condon favoured) vibronic resonances within the overall $S_1 \leftarrow S_0$ absorption, and (ii) adiabatic mapping of the skeletal motions induced in this way into the radical products.

3.3 σ vs π substituent effects on the N–H bond strength

As fig. 2 showed, σ-substituents like methyl or ethyl cause only modest perturbations of the highest occupied (π) MOs of pyrrole. The present study confirms that the positive inductive effect of an alkyl group stabilises the parent cation (Table 2) and thus (via quantum defect arguments) increases the 3*s* Rydberg contribution to the S_1 state in the vFC region and reduces the $S_1 – S_0$ energy gap – more so when introduced at the 2- (*cf*. the 3-) position. The positive inductive effect also serves to stabilize the ground state radical (*cf*. pyrrolyl) – thereby lowering the N–H bond strength. π-substituents can be expected to have greater impact on quantities like the IP, the $S_1 \leftarrow S_0$ excitation energy and the N–H bond strength, as demonstrated in a recent study of substituent effects on the excitation, ionization and dissociation energies of phenols.[29] Here we seek to quantify such π-perturbations in the case of pyrroles, using DFT methods to calculate these values for the case of classic electron donating (MeO) and withdrawing (CN) groups, in both the 2- and 3-positions, as well as for pyrrole, 2-EP and 2,4-DMP. As Table 2 shows, the present calculations reproduce the experimental IP and D_0(N–H) values for pyrrole very well, and the trends (and the magnitudes) of the shifts in N–H bond strength upon alkyl substitution.

The effects of the π-substituents are more dramatic. Neither the identity (CN or MeO) nor the position of the substituent changes the energetic ordering of the HOMO–1, HOMO,

LUMO and LUMO+1 relative to that found in pyrrole, as illustrated in fig. 8. Both substituents have substantial, but predictable, effects on the first IP: an electron donating group (EDG) like MeO stabilizes the parent cation and thus reduces the IP (see Table 2); any distinction between 2- and 3-substitution is muted by the delocalisation of the π HOMO across these positions. (Inspection of the HOMO–1 orbitals suggests that the difference between the second IPs of 2- and 3-methoxypyrrole will be much greater). The converse arguments apply in the case of an electron withdrawing group (EWG) like CN, which destabilises the parent cation and increases the first IP of both the 2- and 3-isomers (*cf.* pyrrole). As noted earlier (fig. 1), the LUMO has substantial N(3s) character in the vFC region but evolves into a σ* antibonding orbital with increasing R_{N-H}. Thus the S_1 state can be viewed as the (valence contaminated) first member of a Rydberg series that converges to the first IP, and quantum defect arguments imply that substituent induced shifts in the first IP should be reflected in the S_1 state energy. As Table 2 shows, these expectations are borne out by the present calculations: the $\Delta E(S_1–S_0)$ vertical excitation energies in the methoxy- and cyanopyrroles are predicted to be, respectively, smaller and greater than that of bare pyrrole. Such considerations account for the predicted shifts in $S_1–S_0$ absorption upon substitution, but offer little insight into the likely slope of the S_1 potential at large R_{N-H}. The present calculations (Table 2) show that MeO substitution leads to a substantial reduction in D_0(N–H), whereas CN substitution causes only a small increase in N–H bond strength. The former is readily understandable; the extended delocalisation afforded by the EWG stabilizes the ground state radical, thereby reducing D_0(N–H).

4. CONCLUSIONS

Following recent studies of the ways in which ring substituents allow some passive control of the fragmentation dynamics of phenols,[28] this article presents a combined experimental (H (Rydberg) atom PTS) and theory (*ab initio* electronic structure calculations) study of the effects of various ring substituents on the photofragmentation dynamics of gas phase pyrroles. The $S_1 \leftarrow S_0$ excitation in pyrrole is electric dipole forbidden, but gains transition probability by vibronic mixing with higher electronic states. The S_1 state is dissociative with respect to N–H bond extension, and the pyrrolyl radical products are formed in a limited number of (non-totally symmetric) vibrational levels, the identities of which reflect the corresponding parent modes that provide the greatest vibronic enhancement at the relevant photoexcitation wavelength.[15] Introducing a σ-perturber (*e.g.* an alkyl group) in the 2-position lowers the molecular symmetry, and the S_1–S_0 transition probability increases. The N–H bond weakens. The radical products are again formed in a limited range of vibrational levels, but these now all involve in-plane (*a′*) ring-breathing motions, consistent with Franck-Condon expectations given the change in equilibrium geometry upon $\sigma^* \leftarrow \pi$ excitation. π-perturbers are predicted to cause relatively greater changes in N–H bond strength, particularly in the case of an electron withdrawing group like methoxy – for which 2- or 3-substitution is calculated to cause a ~10% reduction in D_0(N–H).

ACKNOWLEDGEMENTS

The authors gratefully acknowledge: financial support from EPSRC (programme grant EP/G00224X) and the Marie Curie Initial Training Network ICONIC (contract agreement no. 238671), and the many and varied contributions of J.N. Harvey, A.M. Wenge, K.N. Rosser and J.A. Smith to the work reported here.

Supporting Information Available

(i) Unrelaxed CASPT2(10/10)/aug(N)-AVTZ PECs for 2,4-DMP plotted as a function of $R_{N–H}$; (ii) Plot of photolysis photon energy (E_{phot}) *vs*. $TKER_{max}$ for 2-EP, with a best-fit line of unit gradient superimposed. The *y*-intercept of this plot yields an N–H bond dissociation energy, D_0[2-EPyl–H] = 31650±50 cm^{-1}; (iii) TKER spectra derived from H atom TOF spectra recorded following photolysis of 2,4-DMP at λ_{phot} = 273.373, 268 and 264 nm, along with a plot of E_{phot} *vs*. $TKER_{max}$, with a best-fit line of unit gradient superimposed. The *y*-intercept of this plot yields an N–H bond dissociation energy, D_0[2,4-DMPyl–H] = 31200±50 cm^{-1}; (iv) Lists of anharmonic wavenumbers for the pyrrolyl, *syn*-2-EPyl and 2,4-DMPyl radicals along with their corresponding symmetries in C_{2v} (pyrrolyl) and C_s (2-EPyl and 2,4-DMPyl) computed at the DFT/B3LYP/6-311+G(*d*,*p*) level of theory. This information is available free of charge via the internet at http://pubs.acs.org.

Table 1

EOM-CCSD vertical excitation energies and oscillator strengths for the first four singlet excitations in pyrrole, *anti*-2-ethylpyrrole and 2,4-dimethylpyrrole.

Transition	Pyrrole		*anti*-2-ethylpyrrole		2,4-dimethylpyrrole	
	Vertical energy / eV	Oscillator Strength / *f*	Vertical Energy / eV	Oscillator Strength / *f*	Vertical Energy / eV	Oscillator Strength / *f*
S_1–S_0	5.28	0.0000	5.04	0.0044	4.90	0.0019
S_2–S_0	6.00	0.0240	5.69	0.00002	5.54	0.0012
S_3–S_0	6.11	0.0965	5.91	0.0102	5.73	0.0218
S_4–S_0	6.47	0.0007	6.29	0.1991	6.18	0.1447

Table 2

Zero-point corrected ionization potentials (IPs) and N–H bond strengths energies (D_0(N–H)) for pyrrole, *gauche*-2-ethylpyrrole (forming *syn*-2-ethylpyrrolyl), 2,4-dimethylpyrrole, 2- and 3-methoxypyrrole and 2- and 3-cyanopyrrole, calculated at the DFT/B3LYP/6-311+G(*d*, *p*) level of theory with the Gaussian 09 computational package. Also listed are the $S_1 \leftarrow S_0$ vertical excitation energies ($\Delta E(S_1–S_0)$) calculated by TD-DFT at the same level of theory. The corresponding experimental values (where available) are listed in parentheses.

	IP / cm^{-1}	D_0(N–H) / cm^{-1}	$\Delta E(S_1–S_0)$ / cm^{-1}
pyrrole	65540 (66200±25)[30]	32020 (32850±40)[15]	39940
2-ethylpyrrole	61230	30410 (31650±50)	37770
2,4-dimethylpyrrole	59490	29820 (31200±50)	37070
2-methoxypyrrole	57970	28310	36660
3-methoxypyrrole	58590	28930	36130
2-cyanopyrrole	70690	32640	43080
3-cyanopyrrole	71270	32830	43340

Figure 1

Unrelaxed PECs for the ground and first two excited singlet states of pyrrole plotted as a function of $R_{N–H}$, calculated at the CASPT2(10/10)/aug(N)-AVTZ level of theory.

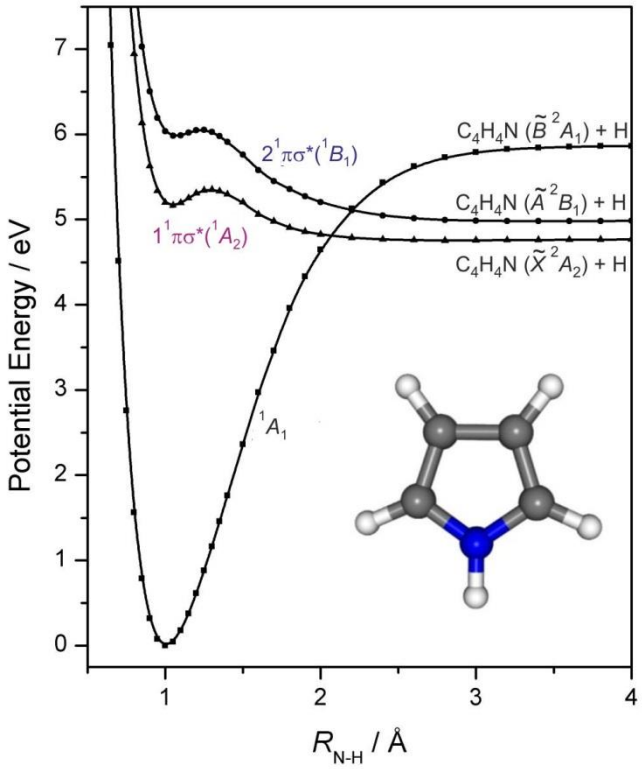

Figure 2

Highest occupied and lowest unoccupied CASSCF molecular orbitals of pyrrole, 2,4-dimethylpyrrole and 2-ethylpyrrole (*anti*-conformer shown for ease of display) arranged in order of increasing energy (from bottom to top). The dominant orbital promotions involved in the various S_n–S_0 (n = 1-4) transitions are indicated.

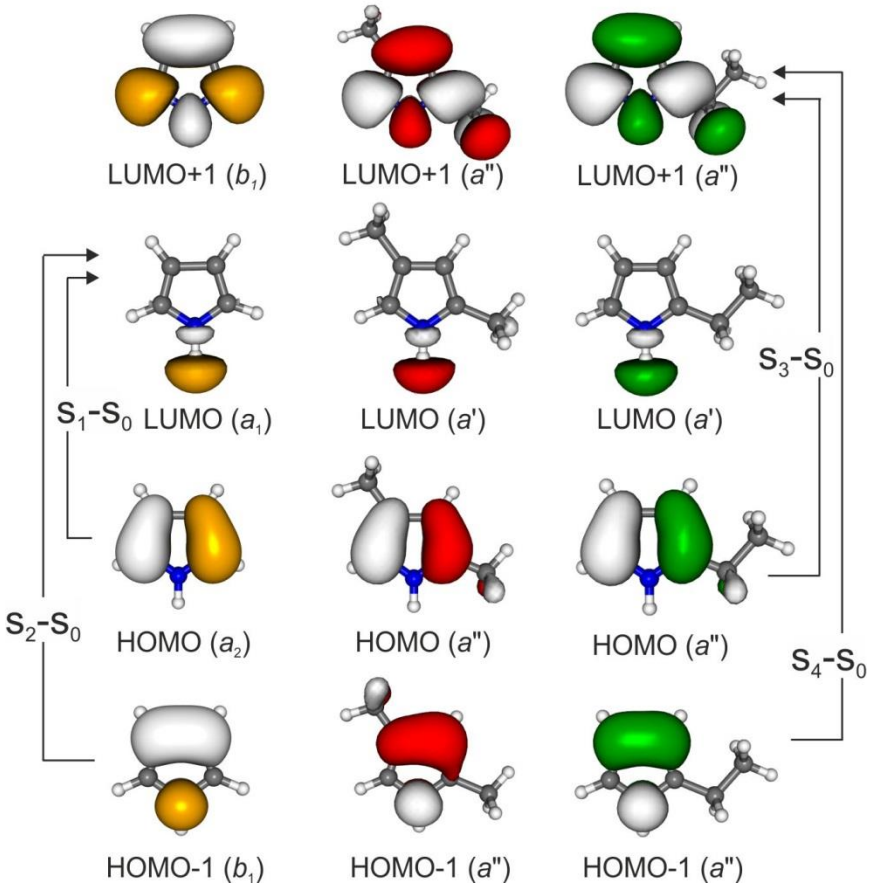

Figure 3

Plots showing relative energies of the different conformers of 2-ethylpyrrole in the S_0 and S_1 states (upper panel), and of the 2-ethylpyrrolyl radical in its ground (D_0) electronic state (lower panel). The dihedral angle ϕ is defined with respect to rotation about the C(2)–CH_2CH_3 bond, with ϕ = 0° when the terminal CH_3 eclipses the N atom as shown in the Newman projections.

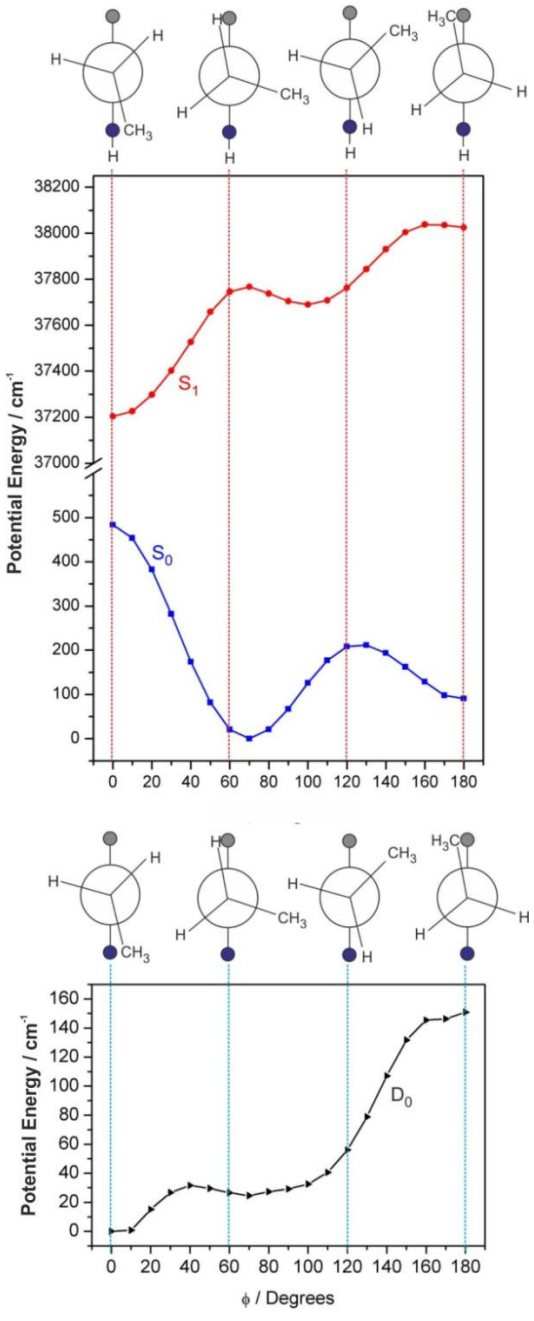

Figure 4

TKER spectra derived from H atom TOF spectra recorded following photolysis of 2-ethylpyrrole at λ_{phot} = (a) 260, (b) 257 and (c) 246 nm.

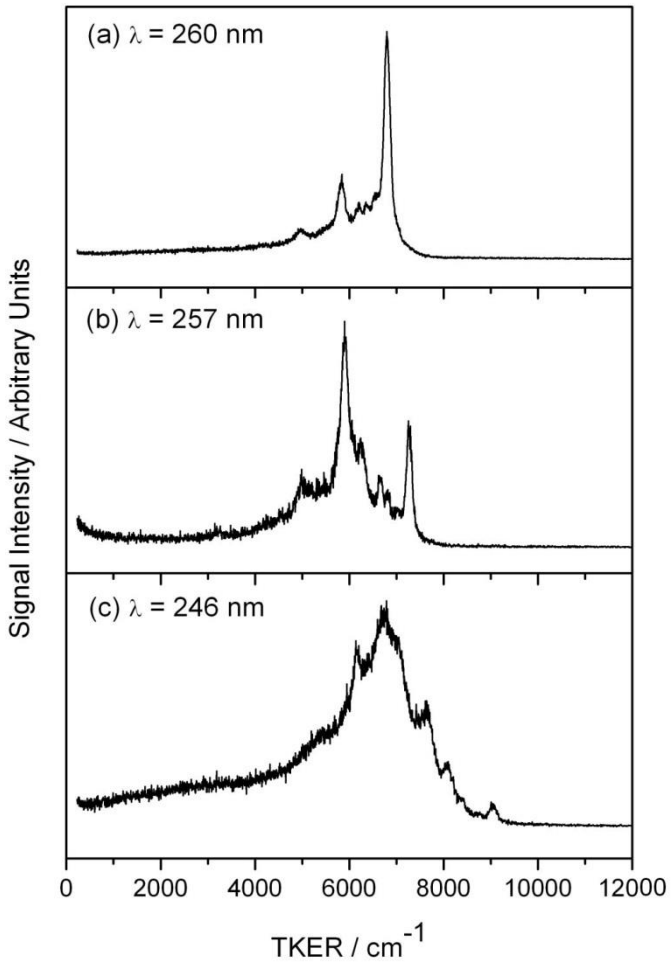

Figure 5

E_{int} spectra of the 2-ethylpyrrolyl products arising in the photolysis of 2-ethylpyrrole at λ_{phot} = (a) 263, (b) 260, (c) 257, (d) 255, (e) 250 and (f) 248 nm.

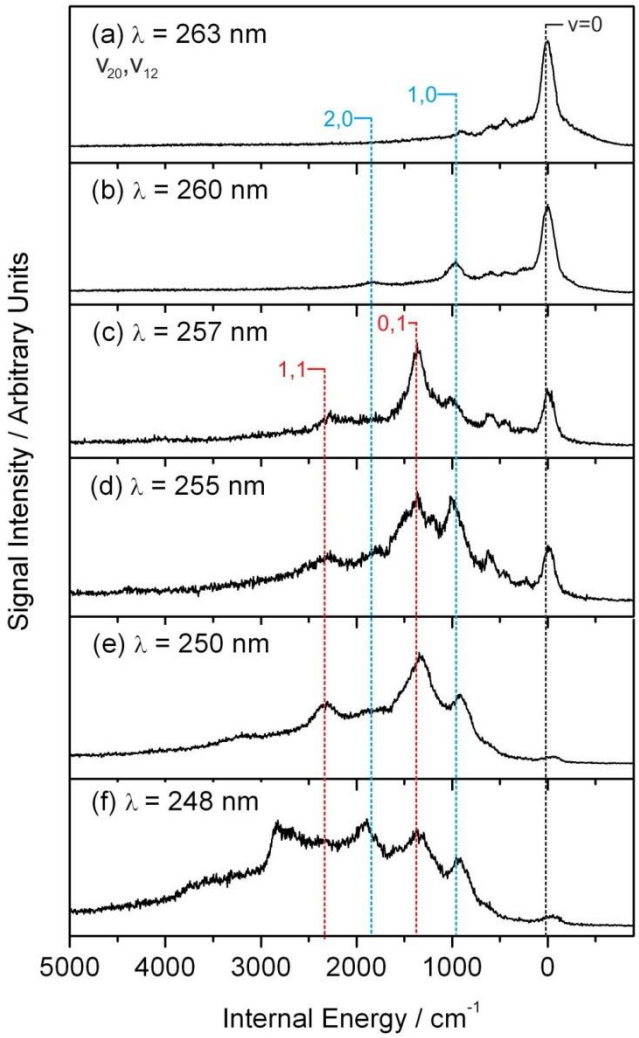

Figure 6

Nuclear motions associated with the various product vibrations identified in the TKER and E_{int} spectra following photolysis of 2-ethylpyrrole and 2,4-dimethylpyrrole.

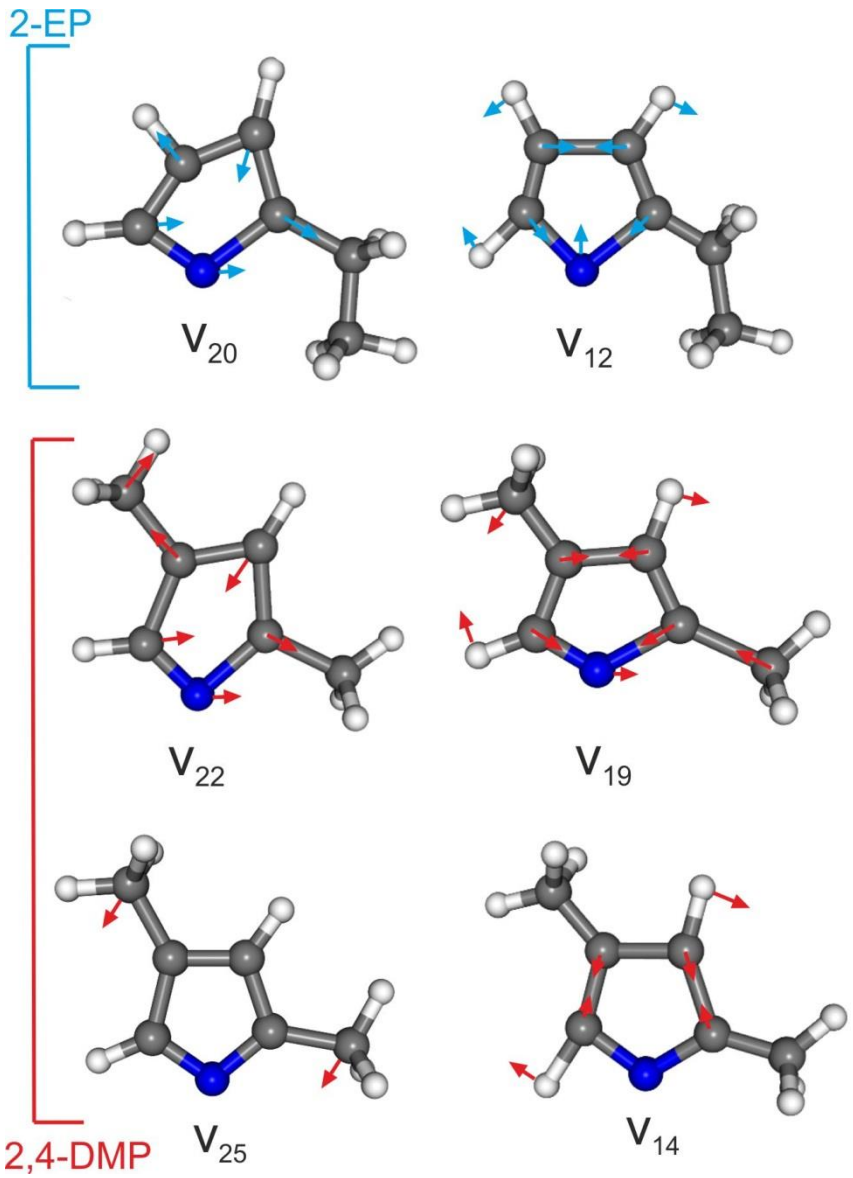

Figure 7

E_{int} spectra of the 2,4-dimethylpyrrolyl products arising in the photolysis of 2,4-dimethylpyrrole at (a) 273.373, (b) 271, (c) 269, (d) 266 and (e) 264 nm.

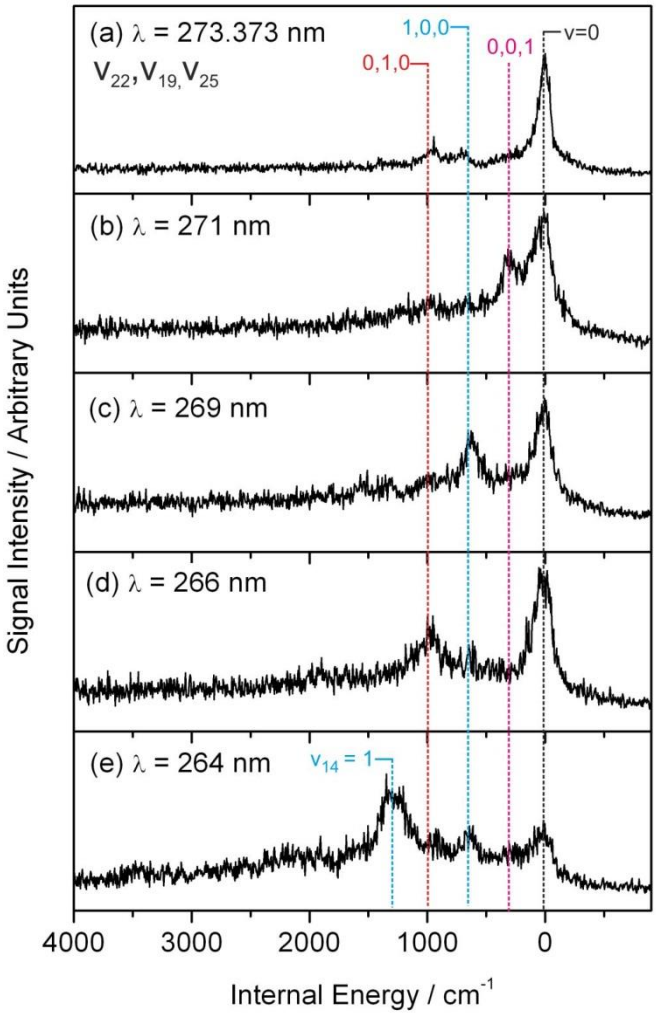

Figure 8

Highest occupied and lowest unoccupied DFT molecular orbitals of pyrrole, 2- and 3-methoxypyrrole and 2- and 3-cyanopyrrole.

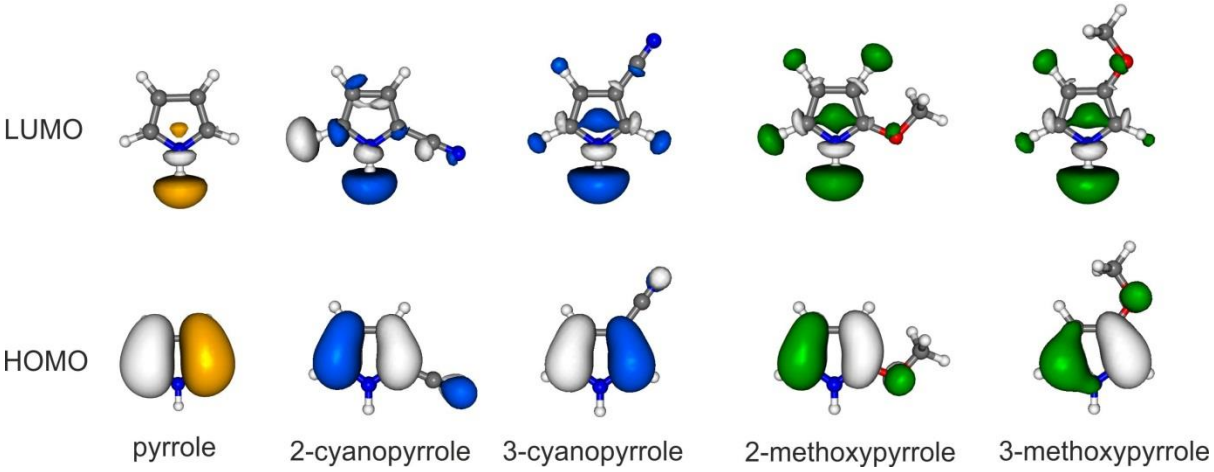

Table of Contents Graphic

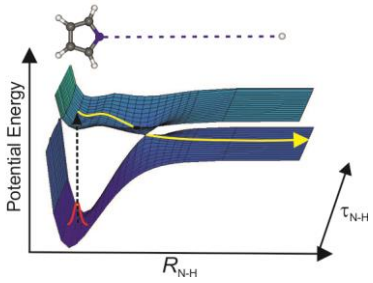

References

1. Ashfold, M.N.R.; Cronin, B.; Devine, A. L.; Dixon, R.N.; Nix, M.G.D. The Role of πσ* Excited States in the Photodissociation of Heteroaromatic Molecules. *Science* **2006**, *312*, 1637-1640.
2. Ashfold, M.N.R.; Devine, A.L.; Dixon, R.N.; King, G.A.; Nix, M.G.D.; Oliver, T.A.A. Exploring Nuclear Motion Through Conical Intersections in the UV Photodissociation of Phenols and Thiophenol. *Proc. Natl. Acad. Sci.* **2008**, *105*, 12701-12706.
3. Ashfold, M.N.R.; King, G.A.; Murdock, D.; Nix, M.G.D.; Oliver, T.A.A.; Sage, A.G. πσ* Excited States in Molecular Photochemistry. *Phys. Chem. Chem. Phys.* **2010,** *12*, 1218-1238.
4. Takahashi, K.; Nihira, T. One-Pot Synthesis and Redox Properties of Conjugation-Extended 4,4′-Bipyridines and Related Compounds. New Ligands Consisting of a Heterocyclic Three-Ring Assembly. *Bull. Chem. Soc. Jpn.*, **1992**, *65* , 1855-1859.
5. Nix, M.G.D.; Devine, A.L.; Cronin, B.; Ashfold, M.N.R. Ultraviolet Photolysis of Adenine: Dissociation via the $^{1}\pi\sigma^{*}$ State. *J. Chem. Phys.* **2007**, *126*, 124312.
6. Perun, S.; Sobolewski, A.L. ; Domcke, W. Photostability of 9H-Adenine: Mechanisms of the Radiationless Deactivation of the Lowest Excited Singlet States. *Chem. Phys.* **2005**, *313*, 107-112.
7. Wells, K.L.; Hadden, D.J.; Nix, M.G.D.; Stavros, V.G. Competing πσ* States in the Photodissociation of Adenine. *J. Phys. Chem. Letts.* **2010**, *1*, 993-996.
8. Wells, K.L.; Roberts, G.M.; Stavros, V.G. Dynamics of H-loss in Adenine via the $^{1}\pi\sigma^{*}$ State Using a Combination of ns and fs Laser Spectroscopy**.** *Chem. Phys. Letts.* **2007**, *446*, 20-24.

9. Blank, D.A.; North, S.W.; Lee, Y.T. The Ultraviolet Photodissociation Dynamics of Pyrrole. *Chem. Phys.* **1994**, *187*, 35-47.

10. Sobolewski, A.L.; Domcke, W.; Dedonder-Lardeux, C.; Jouvet, C. Excited-State Hydrogen Detachment and Hydrogen Transfer Driven by Repulsive $^1\pi\sigma^*$ States: A New Paradigm for Non-radiative Decay in Aromatic Biomolecules. *Phys. Chem. Chem. Phys.* **2002**, *4*, 1093-1100.

11. Vallet, V.; Lan, Z.G.; Mahapatra, S.; Sobolewski, A.L.; Domcke, W. Photochemistry of pyrrole: Time-dependent Quantum Wavepacket Description of the Dynamics at the σ^*-S_0 Conical Intersections. *J. Chem. Phys.* **2005**, *123*, 144307.

12. Roos, B.O.; Malmqvist, P.A.; Molina, V.; Serrano-Andres, L.; Merchan, M. Theoretical Characterization of the Lowest-Energy Absorption Band of Pyrrole. *J. Chem. Phys.* **2002**, *116*, 7526-7536.

13. Wei, J.; Kuczmann, A.; Riedel, J.; Renth, F.; Temps, F. Photofragment Velocity Map Imaging of H Atom Elimination in the First Excited State of Pyrrole. *Phys. Chem. Chem. Phys.* **2003**, *5*, 315-320.

14. Wei, J.; Riedel, J.; Kuczmann, A.; Renth, F.; Temps, F. Photodissociation Dynamics of Pyrrole: Evidence for Mode Specific Dynamics from Conical Intersections. *Farad. Discuss.* **2004**, *127*, 267-282.

15. Cronin, B.; Nix, M.G.D.; Qadiri, R.H.; Ashfold, M.N.R. High Resolution Photofragment Translational Spectroscopy Studies of the Near Ultraviolet Photolysis of Pyrrole. *Phys. Chem. Chem. Phys.* **2004**, *6*, 5031-5041.

16. Rubio-Lago, L.; Zaouris, D.; Sakellariou, Y.; Sofikitis, D.; Kitsopoulos, T.N.; Wang, F.; Yang, X.; Cronin, B.; Devine, A.L.; King, G.A.; *et al.* Photofragment Slice Imaging Studies of Pyrrole and the Xe-pyrrole Cluster. *J. Chem. Phys.* **2007**, *127*, 064306.

17. Lippert, H.; Ritze, H.H.; Hertel, I.V.; Radloff, W. Femtosecond Time-Resolved Hydrogen-Atom Elimination from Photoexcited Pyrrole Molecules. *Chem. Phys. Chem.* **2004**, *5*, 1423-1427.

18. Montero, R.; Peralta Conde, A.; Ovejas, V.; Fernandez-Fernandez, M.; Castano, F.; Vazquez de Aldana, J.R.; Longarte, A. Femtosecond Evolution of the Pyrrole Molecule Excited in the Near Part of its UV Spectrum. *J. Chem. Phys.* **2012**, *137*, 064317.

19. Roberts, G.M.; Williams, C.A.; Yu, H.; Chatterley, A.S.; Young, J.D.; Ullrich, S.; Stavros, V.G. Probing Ultrafast Dynamics in Photoexcited Pyrrole: Timescales for $^1\pi\sigma^*$ Mediated H-Atom Elimination. *Farad. Discuss.* **2013**, *163*, DOI 10.1039/C2FD20140B

20. Cronin, B.; Devine, A.L.; Nix, M.G.D.; Ashfold, M.N.R. Near Ultraviolet Photolysis of Deuterated Pyrrole. *Phys. Chem. Chem. Phys.* **2006**, *8*, 3440-3445.

21. Gianola, A.J.; Ichino, T.; Hoenigman, R.L.; Kato, S.; Bierbaum, V.M.; Lineberger, W.C. Thermochemistry and Electronic Structure of the Pyrrolyl Radical**.** *J. Phys. Chem. A* **2004**, *108*, 10326-10335.

22. Saita, K.; Nix M.G.D.; Shalashilin, D. Simulation of Ultrafast Photodynamics of Pyrrole with the Help of Multiconfigutational Ehrenfest Method. (submitted).

23. Barbatti, M.; Pittner, J.; Pederzoli, M.; Werner, U.; Mitric, R.; Bonacic-Koutecky, V.; Lischka, H. Non-adiabatic dynamics of pyrrole: Dependence of Deactivation Mechanisms on the Excitation Energy. *Chem. Phys.* **2010**, *375*, 26-34.

24. Schnieder, L.; Meier, W.; Welge, K.H.; Ashfold, M.N.R.; Western, C.M. Photodissociation Dynamics of H_2S at 121.6 nm and a Determination of the Potential Energy Function of SH($A^2\Sigma^+$). *J. Chem. Phys.* **1990**, *92*, 7027-7037.

25. Frisch, M.J.; Trucks, G.W.; Schlegel, H.B.; Scuseria, G.E.; Robb, M.A.; Cheeseman, J.R.; Scalmani, G.; Barone, V.; Mennuchi, B.; Petersson, G.A.; *et al*. *Gaussian 09*, revision B.01; Gaussian Inc.: Wallingford, CT, 2010.

26. Werner, H.-J.; Knowles, P.J.; Manby, F.R.; Schütz, M.; Celani,P.; Knizia, G.; Korona, T.; Lindh, R.; Mitrushenkov, A.; Rauhut, G.; *et al*. *MOLPRO*, University of Cardiff: Cardiff, U.K., 2010.

27. Runau, R.; Peyerimhoff, S. D.; Buenker, R. J. *Ab Initio* Study of the Photodissociation of Ammonia. *J. Mol. Spectrosc.***1977**, *68*, 253-268.

28. Cronin, B.; Nix, M.G.D.; Devine, A.L.; Dixon, R.N.; Ashfold, M.N.R. High Resolution Photofragment Translational Spectroscopy Studies of the Near Ultraviolet Photolysis of 2,5-Dimethylpyrrole. *Phys.Chem. Chem. Phys.* **2006**, *8*, 599-612.

29. Karsili, T.N.V.; Wenge, A.M.; Harris, S.J.; Murdock, D.; Harvey, J.N.; Dixon, R.N.; Ashfold, M.N.R. O–H Bond Fission in 4-Substituted Phenols: S_1 State Predissociation Viewed in a Hammett-like Framework. *Chem. Sci.* **2013**, *4*, 2434-2446.

30. Cooper, C.D.; Williamson, A.D.; Miller, J.C.; Compton, R.N. Resonantly Enhanced Multiphoton Ionization of Pyrrole, N-Methyl Pyrrole and Furan. *J. Chem. Phys.* **1980**, *73*, 1527-1537.